A reactive empirical bond order (REBO) potential for hydrocarbon–oxygen interactions

2004 J. Phys.: Condens. Matter 16 7261

(http://iopscience.iop.org/0953-8984/16/41/008)

INSTITUTE OF PHYSICS PUBLISHING JOURNAL OF PHYSICS: CONDENSED MATTER

J. Phys.: Condens. Matter **16** (2004) 7261–7275 PII: S0953-8984(04)78963-8

A reactive empirical bond order (REBO) potential for hydrocarbon–oxygen interactions

Boris Ni[1], **Ki-Ho Lee**[2] **and Susan B Sinnott**[2,3]

[1] Department of Chemistry, McMaster University, Hamilton, ON, L8S 4M1, Canada
[2] Department of Materials Science and Engineering, University of Florida, Gainesville, FL 32611-6400, USA

E-mail: sinnott@mse.ufl.edu

Received 5 April 2004, in final form 19 August 2004
Published 1 October 2004
Online at stacks.iop.org/JPhysCM/16/7261
doi:10.1088/0953-8984/16/41/008

Abstract

The expansion of the second-generation reactive empirical bond order (REBO) potential for hydrocarbons, as parametrized by Brenner and co-workers, to include oxygen is presented. This involves the explicit inclusion of C–O, H–O, and O–O interactions to the existing C–C, C–H, and H–H interactions in the REBO potential. The details of the expansion, including all parameters, are given. The new, expanded potential is then applied to the study of the structure and chemical stability of several molecules and polymer chains, and to modelling chemical reactions among a series of molecules, within classical molecular dynamics simulations.

1. Introduction

The reactive empirical bond order (REBO) potential for hydrocarbons developed by Brenner and co-workers [1–3] and based on potentials first introduced and parametrized by Abell [4] and Tersoff [5–8] has been used extensively to study numerous problems, including chemical reactions at surfaces [9–21], nanoindentation and atomic-scale friction [22–28], and the deformation of carbon nanotubes [29–33]. This potential is many bodied, classical, and empirically derived by fitting to data sets from experiments and *ab initio* calculations. It therefore does not treat electrons explicitly or include any quantum effects. When the results of the REBO potential have been compared to more accurate *ab initio* or tight-binding methods, it has been shown to always be qualitatively accurate and sometimes quantitatively accurate. For instance, the REBO predicts association potentials for $H + CH_3$ and H + diamond (111) that are significantly smaller than *ab initio* values because of the potential's shorter range [34]. However, within the potential cut-off, the predicted association potentials are similar to the

[3] Author to whom any correspondence should be addressed.

ab initio values. When molecular clusters are deposited on surfaces using the REBO potential and a non-orthogonal, order (N) tight-binding method, the overall behaviour of thin-film nucleation was predicted to be the same with both methods [21]. However, the overall amount of cluster-atom adhesion on the surface and the structure of the nucleated start of the thin film was not the same in the two methods [21]. Additional studies where the results of simulations using the Tersoff and Brenner REBO potentials were compared with the results of experiments or more rigorous theoretical approaches generally show that they provide good descriptions of a wide range of mechanical, chemical, and structural properties of materials [35–42].

Despite these limitations, the REBO potential is still used extensively. This is because, unlike molecular mechanics methods, it allows for bond breaking and bond formation to occur over the course of a simulation and is able to model large systems (tens-to-hundreds of thousands of atoms) on standard workstations for relatively long times (tens to hundreds of picoseconds). Therefore, it still finds utility today to study problems that rely on large numbers of atoms in simulations that would be computationally expensive or impossible to model with tight-binding methods or first-principles approaches.

The form of the potential is as follows:

$$E_{\mathrm{b}} = \sum_{i} \sum_{j(>i)} [V^{\mathrm{R}}(r_{ij}) - b_{ij} V^{\mathrm{A}}(r_{ij})] \tag{1}$$

where E_{b} is the chemical binding energy, $V^{\mathrm{R}}(r_{ij})$ is a pairwise term that models core–core and electron–electron repulsive interactions, $V^{\mathrm{A}}(r_{ij})$ is a pairwise term that models core–electron attractive interactions, r_{ij} is the distance between nearest-neighbour atoms i and j, and b_{ij} is a many-body, bond order term that depends on the number and types of neighbours and the bond angles. The advantage of this potential form is that it incorporates much of the physics and chemistry involved in covalent bonding, such as core–electron and electron–electron interactions and many-body effects, and allows for bond breaking and bond formation to occur in a realistic manner. The disadvantage of this potential form is that it is purely empirical and does not include electronic effects or treat electrons explicitly.

The original REBO potential for hydrocarbons [1] has been extended to include F [43, 44] and Si [39, 40, 45], while the second-generation version of the REBO potential for hydrocarbons [3] has been extended to include F [46] and long-range interactions for hydrocarbon systems [47, 48]. In this work, we present an extension of the second-generation version of the REBO potential for hydrocarbons [3] to include oxygen. This development allows for the consideration of chemical interactions among C, H, and O atoms, including covalent bond formation and bond breaking during the course of atomistic Monte Carlo or molecular dynamics (MD) simulations. While this work focuses on covalent bond rupture and formation, it also lays the foundation for future extensions to include long-range interactions, as was done in [45] and [47].

The rest of this paper outlines the fitting procedures used in extending the REBO and discusses its use in some representative applications.

2. Fitting procedure for adding O at the H–C REBO potential

The approach for developing the new H–C–O potential is as follows. First, the parameters and functional forms for C–C, C–H, and H–H interactions are left the same as in [3]. In addition, all of the functional forms used for the extended potential for C–O, O–H, and O–O interactions are the same as those used for the second-generation REBO potential for hydrocarbons [3]. Let us consider the case of the pairwise interaction terms first. These functional forms are as

follows:

$$V^{\mathrm{R}}(r) = f^{\mathrm{c}}(r)(1 + Q/r)A\mathrm{e}^{-\alpha r} \tag{2}$$

$$V^{\mathrm{A}}(r) = f^{\mathrm{c}}(r) \sum_{n=1,3} B_n \mathrm{e}^{-\beta_n r} \tag{3}$$

where $f^{\mathrm{c}}(r)$ is a function that is used to limit the range of covalent interactions to nearest neighbours, r is the interatomic distance, and Q, A, B_n, α, and β_n are parameters that are fit to a dataset. These terms are then corrected by the bond order value, which is given by the following equation [3]:

$$\bar{b}_{ij} = \tfrac{1}{2}[b_{ij}^{\sigma-\pi} + b_{ji}^{\sigma-\pi}] + b_{ij}^{\pi}. \tag{4}$$

The functions $b_{ij}^{\sigma-\pi}$ and $b_{ji}^{\sigma-\pi}$ depend on the local coordination and bond angles for atom i and j, respectively, while the function b_{ij}^{π} is

$$b_{ij}^{\pi} = \prod_{ij}^{\mathrm{RC}} + b_{ij}^{\mathrm{DH}} \tag{5}$$

where $\prod_{ij}^{\mathrm{RC}}$ depends on whether a bond between atoms i and j has radical character and is part of a conjugated system, while b_{ij}^{DH} depends on the dihedral angle for double bonds [3]. Hence, in the REBO potential, atomic bonding is determined only from local bonding neighbours and non-local conjugation that is influenced by the coordination of the nearest-neighbour atoms. This allows the influence of atomic rehybridization on the binding energy to change as chemical bonds break and reform over the course of a simulation.

The first term in equation (4) is expressed as follows [3]:

$$b_{ij}^{\sigma-\pi} = \left[1 + \sum_{k(\neq i,j)} f_{ik}^{\mathrm{c}}(r_{ik})G(\cos(\theta_{ijk}))\mathrm{e}^{\lambda_{ijk}} + P_{ij}(N_i^{\mathrm{C}}, N_i^{\mathrm{H}}, N_i^{\mathrm{O}})\right]^{-\frac{1}{2}} \tag{6}$$

where the subscripts refer to the atoms, the function $f^{\mathrm{c}}(r)$ limits the interactions to nearest neighbours only, the function P represents a bicubic spline, and the quantities N_i^{C}, N_i^{H}, and N_i^{O} represent the number of C, H, and O atoms, respectively, that are the nearest neighbours of atom i [3]. λ is a parameter that is designed to prevent attraction force in some specific situations, or, in other words, it is a fitting parameter used to describe three-body intermediate states. Lastly, the term $G(\cos(\theta))$ is an angular function that is discussed in detail below.

The strategy of parametrizing the extended potential is the same as that taken by Brenner [1–3] for pure hydrocarbon systems. First we obtain the sets of parameters Q, A, B, α, and β for the repulsive and attractive terms of potential that involve O. The parameters are developed so that the potential correctly reproduces a range of equilibrium distances and the bond energies for various O–O, C–O, and O–H bonds. This means that the desired parametrized functions should be equally able to describe the bond length, energy, and force constant of a C–O bond in, for example, methanol and acetaldehyde. The potential energy function also has to demonstrate the tendency of increasing of bond energy and force constants with shortening of the bond length. All the differences in the energies, bond lengths, and force constants for particular bonds in different molecules are ruled by the bond order term, b_{ij}. Thus, a secondary tuning of the potential energies for specific molecules involves the parametrization of this bond order term according to the specific environment of each atom connected by the bond.

Unlike the approach taken by Brenner, however, we fit the extended C–O, O–O, and O–H potential functions to values obtained exclusively by high-level, quantum chemical calculations rather than experimental bond energies and force constant values. Specifically, the density functional theory (DFT) method with the B3LYP exchange–correlation potential and 6-311G*

basis set in Gaussian 98 was used [49]. We have chosen to fit to a theoretically determined database because of the ease in obtaining information on any kind of species and because of the precision and reliability of modern quantum chemical methods. More importantly, the quantum chemical calculations allow us to obtain values that would be difficult to obtain experimentally. For example, in our fitting procedure we use the energies of symmetrically deformed C–O, O–O, and O–H bonds in CO_2, O_3, and H_2O, in addition to the energies of relaxed configurations.

For the initial parametrization of attractive and repulsive terms of each bond, we picked a few molecules to represent the different types of bonds that are important for H–C–O systems. For a single O–O bond, the bond in the HO–OH molecule was used. For the stronger double O–O bond, the bond in the O_2 molecule was used. For the intermediate strength of conjugate bonding we chose the O–O bond in O_3. The symbols in figure 1(a) illustrate the manner in which the symmetrical deformations of these bonds compare to one another. The C–O single bond was taken from the CH_3–OH molecule, the double C–O bond was taken from the CO_2 molecule, and the triple C–O bond was taken from the CO molecule. The symbols in figure 1(b) illustrate the manner in which the symmetrical deformations of these bonds compare to one another. Finally, the curve for the O–H bond, taken from the H–OOH molecule, is shown in figure 1(c). A complete list of the representative molecules, the calculated minimum energy values for bond energies and bond-lengths, and available experimental values are given in table 1. It should be emphasized that the table lists only the equilibrium bond lengths and bond energies for the molecules shown in figure 1, while the figure also includes the energies of bonds that are extended or contracted relative to their equilibrium positions.

The dissociation bond energies of representative molecules are calculated as the difference between the energy of molecules and the energy of the products after bond cleavage. Because of the inability of the REBO potential to describe the decomposition of molecules into charged ions, only homolytic reactions with radical products were considered in the quantum chemical calculations. Corresponding spin multiplicity was also taken into account in the calculations. All the equilibrium structures were fully optimized and relaxed in the quantum chemical calculations within the Gaussian 98 program until the energy minima were reached.

To fit an analytical function to an arbitrary function given by point values, the number of given points should be bigger than the number of parameters. We therefore made nine single-point scanning calculations of potential energy surfaces (PES) (shown in figure 1) near the equilibrium distance for every type of bond in the representative molecules discussed above. Then parameters for equations (2) and (3) were obtained using the method of least-squares fitting and are shown in table 2. Each potential energy surface obtained by the nine scanning DFT calculations and shown in figures 1(a)–(c) is described to a precision of 10^{-4} by the following six parameters: Q, A, α, b_{ij}, B1, and $\beta 1$. The values of these parameters are given in table 2. The initial guess for the bond order, b_{ij}, was about 1.0, providing a smooth increase with increasing bond energy and decreasing bond length.

To ensure that the final sets of parameters could cover the whole range of energies and bond lengths in different molecules, we next averaged the Q, A, B, α, and β parameters that represent different kinds of bonding. These are given in table 2 in column 'Ave.'. These averaged sets of parameters are then used in all future calculations. The dashed curves in figure 1 show the extrapolated potential energy functions with the given averaged sets of parameters and different values of bond orders. The figure shows slight discrepancies between the equilibrium bond distances predicted by the potential functions (with the averaged set of parameters) and those calculated with DFT (B3LYP). This happens because of the averaging of the parameters from different potential energy surfaces (PESs). For example, it is difficult to precisely fit the PES of HO–OH (the diamond symbols in figure 1(a)) and the PES of the symmetrical deformation

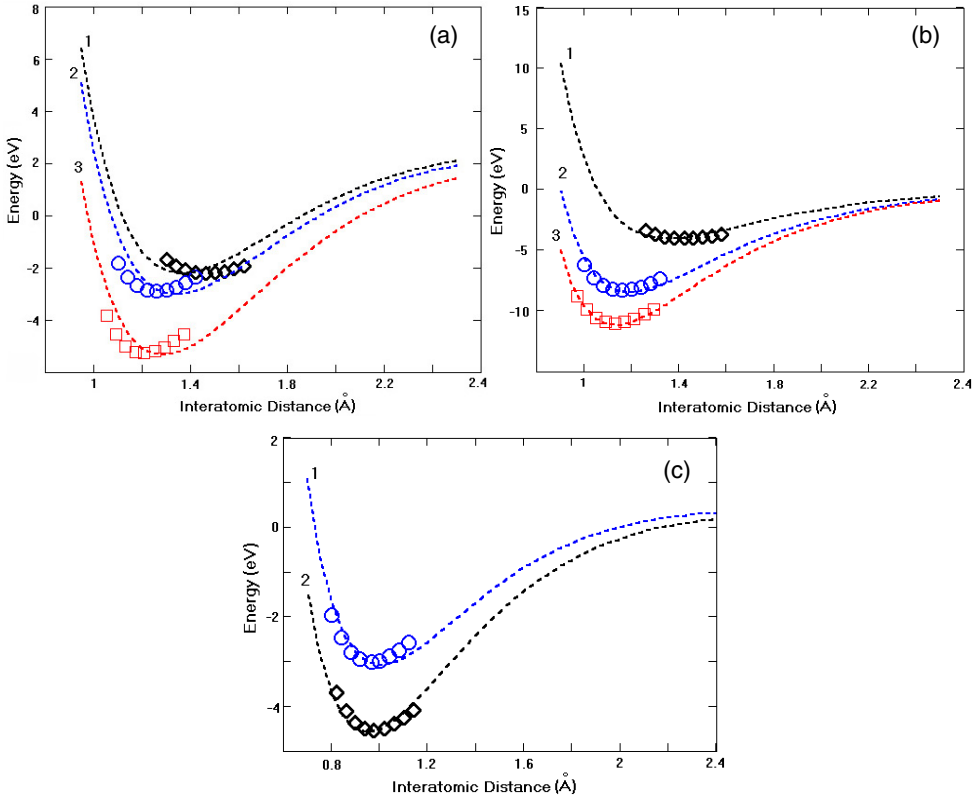

Figure 1. Potential energy surfaces obtained by single-point density functional theory calculations shown by diamond, circle, and square symbols: (a) for different O–O bonds, (b) for different C–O bonds, and (c) for different O–H bonds. The dashed curves represent extrapolated analytical functions with the averaged parameters for attractive and repulsive parts of the potential but different bond orders.

in O–O–O (the circular symbols in figure 1(a)) with the same set of parameters by varying only the bond order because the bond distances in these molecules are quite different from one another (1.464 and 1.258 Å respectively), whereas the bond energies differ slightly from one another (−2.23 and −2.92 eV), as shown in table 1. As a result of this averaging, the range (distribution) of equilibrium bond distances is smaller in the extended REBO potential than in the DFT (B3LYP) calculations. Nevertheless, the trend given by the averaged parameters is correct: the larger the bond energy the shorter the bond length and the higher the force constants. The worst deviation of the predicted equilibrium distance from the one calculated by DFT (B3LYP) does not exceed ∼0.1 Å. For instance, the bond distance for HO–OH given by DFT is 1.464 Å and the one predicted by the potential function is 1.369 Å (both give the same energy of 2.23 eV). In addition, the bond distance predicted by DFT (B3LYP) for O_2 is 1.206 Å and the one predicted by the potential function is 1.279 Å. The PESs for the C–O and O–H bonds are approximated by the averaged parametrized functions much better than for O–O bonds, and provide a good fit for bond distances, bond energies, and curvature of the PESs.

The next step is to allow the bond order to vary to reflect the change in bond lengths and dissociation bond energies in different bonding environments. The bond order value depends on both the coordination of the atoms and the angles between their bonds, as shown in

Table 1. Equilibrium distances and bond energies for O–O, C–O, and O–H bonds in representative molecules taken for initial parametrization. The calculated data are from the DFT calculations, as described in the text. (Experimental values for which there is no reference number (in square brackets) are taken from [50].)

	Bond distance (Å)		Bond energy (eV)	
Name	Calculation	Experiment	Calculation	Experiment
HO–OH	1.463 8	1.480	−2.226	−2.212
O–O–O Symm. deform.	1.257 7	1.278	−2.921[a]	
	OOO angle = 116.8 degrees			
O_2	1.205 6	1.208	−5.281	−5.165
C=O	1.127	1.128 [52]	−11.016	−11.158
O=C=O Symm. deform.	1.160 44	1.162 [52]	−8.358[a]	−5.516
CH_3–OH	1.421 3	1.427	−4.038	−3.903 [53]
O–H	0.975 2	0.971 [52]	−4.544	−4.432
H–O–H Symm. deform.	0.961 8	0.958 [52]	−4.867[a]	−5.160
H–OO–H Symm. deform.	0.964 9	0.960	−3.016[a]	−3.825

[a] Calculated bond energy from symmetrical deformation of bonds (O_3, CO_2, H_2O, H–OO–H).

Table 2. Parameters for analytical functions fit to the potential energy surfaces of individual bonds in representative molecules and their average values.

	O–O bond				C–O bond				O–H bond		
	HO–OH ◇◇	O–O–O ○○	O=O □□	Ave. O–O ----	CH_3–OH ◇◇	O–C–O ○○	C=O □□	Ave. C–O ----	H–OO–H ○○	O–H ◇◇	Ave. O–H ----
Q	0.422	0.392	0.392	0.4065	8.286	9.817	9.293	9.132	0.125	0.122	0.1235
A	688.52	681.96	680.1	685.255	78.193	83.793	81.187	81.058	711.20	723.1	717.150
α	1.183	1.163	1.162	1.173	3.227	3.781	3.654	3.554	1.525	1.731	1.628
b_{ij}	1.00	1.006	1.011		0.94	1.133	1.143		1.003	1.011	
B_1	1095.0	1115.0	1120.0	1105.0	235.06	283.25	285.819	268.04	890.42	878.59	884.504
β_1	1.318	1.332	1.332	1.325	2.214	2.472	2.346	2.344	1.618	1.79	1.704
$D_{\min}$				1.55				1.60			1.30
$D_{\max}$				1.70				1.90			1.70

Table 3. Angular dependence of O–O bond energy calculated for the O_3 molecule.

Θ (deg.)	E (eV)
180.0	−1.152
160.0	−1.687
150.0	−2.123
140.0	−2.510
118.2	−2.921
100.0	−2.384
80.0	−0.187

equation (6). Because of the differences in the natural hybridization of the atomic orbitals of C and O, the angular function for the cases when O is sitting between two bonds is parametrized. We therefore performed calculations of the bond energies in the O_3 molecule with angles varying from 80° to 180°; the results are shown in table 3. The minimum energy corresponds to an angle of 118.2° (the experimental value is 116.8° [50]). The energy values for the different angles between the bonds are used to obtain discrete values of the bond order and

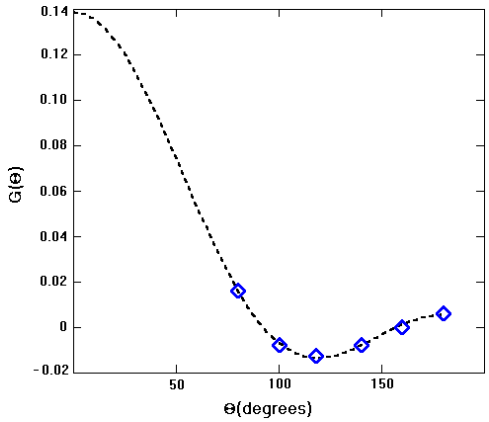

Figure 2. Extrapolated analytic function reflecting the dependence of the bond energy on angle between bonds when oxygen sits at the top of the angle. Fitting points (shown by diamond symbols) are derived from discrete values of the bond order at the given angles.

corresponding values of the angular function using equation (6). The discrete values of the angular function are then interpolated by an analytic function expressed by the formula

$$G(\theta) = a_0 + a_1[a_2 - \cos(\pi/180°\theta)]^2. \tag{7}$$

Parameters for this function are determined using the least-squares method and are found to be $a_0 = -0.014$, $a_1 = 0.07$, and $a_2 = -0.478$. The extrapolated angular function $G(\theta)$ is shown in figure 2.

The function P_{ij} in equation (6) represents the correction of the bond order (and, consequently, the bond energies and bond lengths) due to the specific environment of the atoms in particular molecules. The discrete values of the P_{ij} function, and the corresponding bond energies, have been calculated for different kinds of environments in the various molecules that are shown in table 4. In the table, the first index, m, is the sum of the number of neighbouring C and H atoms and the second index, n, is the number of neighbouring O atoms. The reason for the summation of the number of C and H atoms in the first index is that we did not want to separate the influence of a neighbouring C atom from that of a neighbouring H atom because of their close electronegativity and consequently similar nature of their sigma bonding. For instance, the values of the dissociation energy of the C–O bond in CH_3–OH, CH_3–CH_2–OH, $(CH_3)_2$–CH–OH, and $(CH_3)_3$C–OH are almost exactly the same (around 3.97 eV). Correction of the bond energy due to π orbital conjugation is taken into account in another term (see equation (4)). To ensure that P_{ij} is continuous through its second derivative, we have fit a bicubic spline to the discrete points shown in table 4 and stored the coefficients for faster future simulations.

We preserved the hydrocarbon part of the potential without change. Consequently, C and H atoms that are not surrounded by O atoms are unchanged from the form in [3] and the corresponding cells of the correction function, P, in table 4 are empty. The roles of the C and O atoms in a C–O bond are unequal (unlike the roles of the C atoms in the C–C bond) because of their different electronegativities and valences. The influences of the coordination of the C and O atoms are also unequal. For example, C can make four bonds whereas O can form only two bonds. Therefore, we have to interpolate the P function from both the C and the O sides of the bond separately. For better interpolation of the P function, in some cases we considered species that are unstable (such as the C–O bond in CH_3–O–$(OH)_3$). In table 4,

Table 4. Values at the knots and associated fitting species for the function P used in the carbon–oxygen bond order function. All values and derivatives not listed are equal to zero. A continuous function is created using a bicubic spline determined from these values.

C–O bond					O–C bond				
m	n	Fitting species	E (eV)	$P_{CO}(m,n)$	m	n	Fitting species	E (eV)	$P_{OC}(m,n)$
0	0	C=O	−11.016	−0.390	0	0	CH_3–O	−4.00	0.0
0	1	O=C=O	−5.702	0.109	0	1	CH_3–OOH	−2.890	1.026
0	2	2(OH)–C=O	−4.837	0.177	0	2	CH_3–O–$(OH)_2$	+1.0	19.048
0	3	C–$(OH)_4$	−4.580	0.054	0	3	CH_3–O–$(OH)_3$	+1.0	19.057
1	0	CH–OH Radical	−5.595	0.128	1	0	CH_3–O–CH_3	−3.7846	0.607
1	1	HCO–OH	−4.854	0.173	1	1	CH_3–O–HOH	+1.0	19.057
1	2	CH–$(OH)_3$	−4.797	9.689×10^{-5}	1	2	CH_3–OH–$(OH)_2$	+1.0	19.057
2	0	CH_2–OH	−5.353	0.066	2	0	CH_3–OH_2	+1.0	19.057
2	1	CH_2–$(OH)_2$	−4.291	0.135	2	1	CH_3–OH_2OH	+1.0	19.057
3	0	CH_3–OH	−4.038	0.213	3	0	CH_3–O–H_3	+1.0	19.057

C–C Bond					C–H bond				
m	n	Fitting species	E (eV)	$P_{CC}(m,n)$	m	n	Fitting species	E (eV)	$P_{CH}(m,n)$
0	0	—			0	0	—		
0	1	HOC=COH	−4.643	+0.139	0	1	CH–OH	−3.547	+0.385
0	2	O=COH–COH=O	−3.485	+0.231	0	2	O=CH–OH	−4.451	−0.083
0	3	C_2–6OH	−3.715	-6.253×10^{-3}	0	3	CH–$(OH)_3$	−4.309	−0.224
1	0	—			1	0	—		
1	1	C_2H_2=2O	−3.058	+0.350	1	1	CH_2–OH	−3.846	+0.137
1	2	C_2H_2–4OH	−3.685	-7.662×10^{-5}	1	2	CH_2–$(OH)_2$	−4.350	−0.238
2	0	—			2	0	—		
2	1	C_2H_4–2OH	−3.485	+0.045	2	1	CH_3–OH	−4.325	−0.229
3	0	—			3	0	—		

O–O bond					O–H bond				
m	n	Fitting species	E (eV)	$P_{OO}(m,n)$	m	n	Fitting species	E (eV)	$P_{OH}(m,n)$
0	0	O=O	−5.281	−0.036	0	0	O–H	−4.544	−0.022
0	1	O–O=O	−0.561	0.028	0	1	HOO–H	−3.762	-6.56×10^{-3}
0	2	$(OH)_2$–O–O–$(OH)_2$	+1.0	0.062	0	2	O_2–O–H	+1.0	0.075
0	3	$(OH)_3$–O–O–$(OH)_3$	+1.0 eV	0.071	0	3	O_3–O–H	+2.0	0.082
1	0	HO–OH	−2.226	1.166×10^{-3}	1	0	HO–H	−5.190	−0.019
1	1	HOHO–OHOH	+1.0	0.071	1	1	O–HO–H	+1.0	0.075
1	2	$(OH)_2$–OH–OH–$(OH)_2$	+1.0	0.071	1	2	$(OH)_2$–HO–H	+1.0	0.082
2	0	H_2O–OH_2	+1.0	0.062	2	0	OH_3	+1.0	0.075
2	1	H_2–OHO–OOH–H_2	+1.0	0.071	2	1	HO–H_2O–H	+1.0	0.082
3	0	H_3O–OH_3	+1.0	0.071	3	0	OH_4	+1.0	0.082

this fact is reflected in the positive sign of the bond energy (the +1 eV for this energy is an arbitrary value chosen to ensure a swift decay of the bond).

Table 4. (Continued.)

The values of partial derivatives at the knots					
$\partial P_{CO}(2,2)/\partial m$	0.013	$\partial P_{OC}(2,2)/\partial m$	9.0155	$\partial P_{CC}(2,2)/\partial m$	−0.047
$\partial P_{CO}(2,1)/\partial m$	0.228	$\partial P_{OC}(2,1)/\partial m$	9.7235	$\partial P_{CC}(2,1)/\partial m$	0.000
$\partial P_{CO}(3,1)/\partial m$	0.0425	$\partial P_{OC}(3,1)/\partial m$	9.27	$\partial P_{CC}(3,1)/\partial m$	0.000
$\partial P_{CO}(2,2)/\partial n$	−0.063 95	$\partial P_{OC}(2,2)/\partial n$	9.27	$\partial P_{CC}(2,2)/\partial n$	−0.000 038 31
$\partial P_{CO}(1,2)/\partial n$	0.2835	$\partial P_{OC}(1,2)/\partial n$	9.7235	$\partial P_{CC}(1,2)/\partial n$	0.1155
$\partial P_{CO}(1,3)/\partial n$	−0.0275	$\partial P_{OC}(1,3)/\partial n$	9.0155	$\partial P_{CC}(1,3)/\partial n$	−0.072 6265
$\partial P_{CH}(2,2)/\partial m$	−0.307	$\partial P_{OO}(2,2)/\partial m$	0.0215	$\partial P_{OH}(2,2)/\partial m$	0.04428
$\partial P_{CH}(2,1)/\partial m$	0.000	$\partial P_{OO}(2,1)/\partial m$	0.049	$\partial P_{OH}(2,1)/\partial m$	0.0485
$\partial P_{CH}(3,1)/\partial m$	0.000	$\partial P_{OO}(3,1)/\partial m$	0.034 917	$\partial P_{OH}(3,1)/\partial m$	0.0465
$\partial P_{CH}(2,2)/\partial n$	−0.119	$\partial P_{OO}(2,2)/\partial n$	0.034 917	$\partial P_{OH}(2,2)/\partial n$	0.0465
$\partial P_{CH}(1,2)/\partial n$	−0.0415	$\partial P_{OO}(1,2)/\partial n$	0.049	$\partial P_{OH}(1,2)/\partial n$	0.0485
$\partial P_{CH}(1,3)/\partial n$	−0.3045	$\partial P_{OO}(1,3)/\partial n$	0.0215	$\partial P_{OH}(1,3)/\partial n$	0.044 28

Table 5. Comparison of predicted bond dissociation energies calculated from expanded REBO potential at zero kelvin and measured values. The bond that is dissociated is indicated by a '–'.

	Bond dissociation energy (eV)		Bond length (Å)	
Molecule	C–O–H REBO	Experiment	C–O–H REBO	Experiment
O–O	−5.256	−5.161 ± 0.002[a]	1.286	1.208
HO–OH	−2.795	−2.212 ± 0.043[a]	1.343	1.480
OC–O	−3.591	−5.516 ± 0.004[a]	1.264	1.162[b]
CH_3–OH	−4.126	−3.903[c]	1.350	1.427
CH_3CO–OH	−3.448	−3.903[c]	1.340	1.434
O–H	−4.411	−4.431[a]	0.956	0.971[b]
HO–H	−4.663	−5.160 ± 0.043[a]	0.961	0.958[b]
HOO–H	−3.203	−3.903[b]	0.958	0.970[b]
CH_3O–H	−3.282	−4.527 ± 0.043[a]	0.952	0.956
CH_3COO–H	−3.254	−4.020[a]	0.952	
CH_3CH_2O–H	−3.285	−4.519 ± 0.043[a]	0.952	
C–H	−4.526	−3.504[a]	1.090	1.101[a]
CH_3–H	−4.810	−4.558 ± 0.007[a]	1.089	1.091[a]
CH_3–CH_3	−4.096	−3.816 ± 0.087[a]	1.543	1.541[a]
H–$CH_2C(CH3)_2$	−2.160	−3.712[a]	1.090	

[a] From [49].
[b] From [51].
[c] From [52].

3. Applications of the REBO H–C–O potential

To evaluate the strengths and weaknesses of the extended REBO potential we use it to relax several structures and to model the chemistry that results from selected gas-phase collisions in MD simulations. The simulations numerically integrate Newton's equations of motion with a third-order Nordsieck predictor corrector integration algorithm to track the motion of the atoms with time. The time step used for the integration is 0.2 fs. As a check, selected simulations are run with smaller time steps and in all cases but one (discussed below) the results are identical to the results obtained using the 0.2 fs time step.

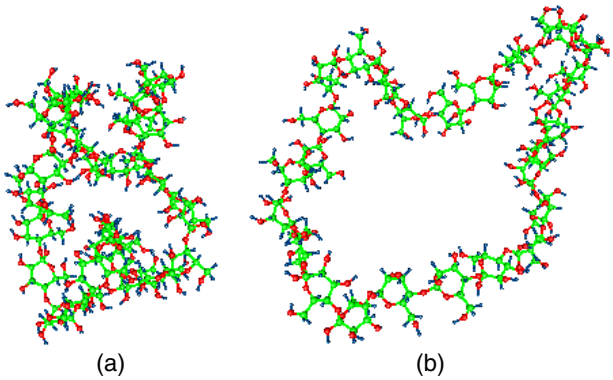

Figure 3. The chain conformations of amylose at (a) 0 ps, and (b) 12 ps after an initial thermostat equilibration at 300 K for 3.2 ps.

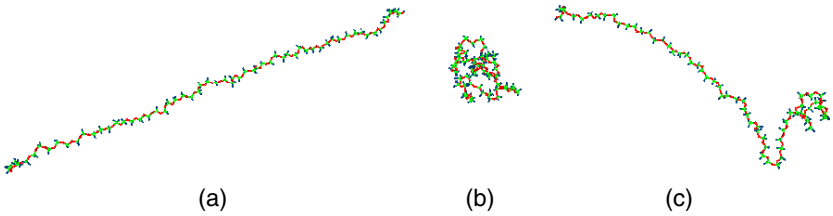

Figure 4. The chain conformations of POM at (a) 0 ps, (b) 4 ps, and (b) 14 ps after an initial thermostat equilibration at 300 K for 3.2 ps.

3.1. Optimization of structure

As a first test of the extended potential, a series of molecules and polymers are examined in MD simulations. The structures of a range of molecules, from diatomics to polymer chains, are optimized using MD simulations. The molecules considered are hydrogen, oxygen, water, methyl radical, methane, ethyl radical, ethane, methanol, ethanol, 1-butanol, 1-octanol, ethyl ether, and n-butyl ether. To start, all the atoms in the molecules are designated as thermostat atoms using a Langevin thermostat [51] and are individually equilibrated for 3.2 ps at 300 K. This equilibration ensures that the systems have appropriate initial conditions for temperature and energy. The thermal energy at 300 K is expressed in kinetic vibrational, rotational, and translational molecular motion. Following equilibration, the molecules are allowed to dynamically evolve without any constraints due to thermostats, i.e., according to purely Newtonian forces, for 50 ps. There is little change in the total energy and appropriate bond lengths and angles are quickly reached and then maintained. Table 5 provides a listing of bond lengths predicted by these equilibration steps and a corresponding comparison to experimental data. The largest increase in the total energy over the course of relaxation is about 3×10^{-3} eV/atom.

To more fully test the robustness of the potential, the polymer chains considered, amylose, polyoxymethylene (POM), and poly(ethylene terephthalate) (PET), are relaxed from initial structures that are far from equilibrium. Figure 3 shows snapshots of the initial structure of amylose and the structure after relaxation. It can be seen that the polymer relaxes significantly from the initial positions. In the case of POM, the chain structure is built by substituting CH_2 in a polyethylene structure with O, causing highly strained bond lengths and angles. As

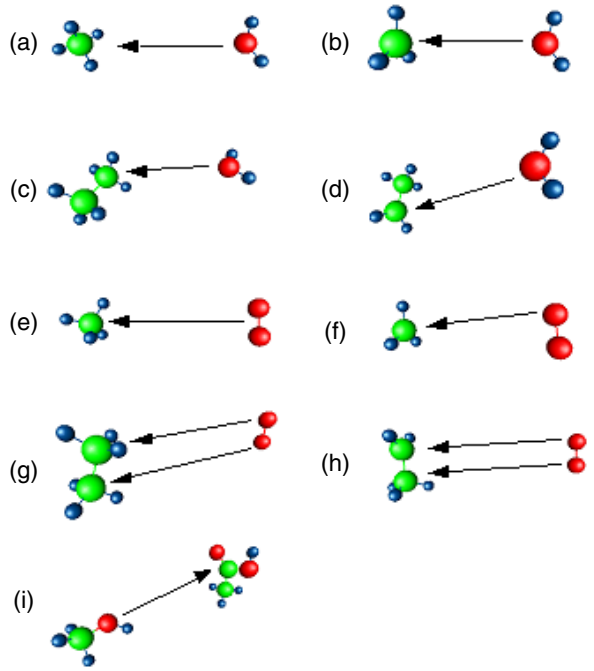

Figure 5. Snapshots of various representative collision tests. (a) H_2O/CH_4; (b) H_2O/CH_3; (c) H_2O/CH_3CH_3; (d) H_2O/CH_3CH_2; (e) O_2/CH_4; (f) O_2/CH_3; (g) O_2/CH_3CH_3; (h) O_2/CH_3CH_2; (i) CH_3OH/CH_3COOH. The blue spheres are hydrogen atoms, the green spheres are carbon atoms, and the red spheres are oxygen atoms. The arrows indicate the target atoms for the cases illustrated in the figure.

a result, the POM chain is initially stretched relative to the fully equilibrated chain. As the system equilibrates the chain contracts and then expands to a less strained structure. Snapshots of the structural relaxation of the POM chain are shown in figure 4. In the case of PET, nine chains arranged in a crystalline configuration are considered. The structure of these chains changes from the initial, highly strained configuration to a more relaxed configuration. It is recognized however, that to appropriately model long-range van der Waals interactions between polymer backbones, the short-ranged REBO potential constructed here needs to be coupled with a long-range potential, such as a Lennard-Jones potential, as is done by us and others elsewhere [47, 48]. Similarly, the short-ranged nature of this extended REBO potential will not allow it to be used alone to characterize hydrogen bonding in water.

In table 5, some calculated bond dissociation energies are shown and compared to measured experimental data. The dissociation of O_2 into its constituent atoms, H_2O into HO + H, and CO_2 into CO + O, and the breaking of the CH_3–OH bond in methanol, all involve bonds that were part of the fitting database and so the good agreement with experimental values is inherent to the construction of the potential. Nevertheless, one may notice the disagreement between fitting values and predicted dissociation bond energies for CO and CO_2 molecules. Instead of -11.016 and -5.702 eV that were set initially for C=O and OC–O bonds (see column 4 in table 4) the calculated dissociation energies are -8.329 and -3.806 eV respectively (see column 4 in table 5). This result is explained by 'non-symmetrical' parametrization taken from each of the carbon and the oxygen atom side (see above). For example, when we tried symmetrical parametrization where the O–C bond energy for a system where the oxygen has

no other neighbours was fit to −11.016 eV (the strength of the C–O bond in CO), the O–C bond in the CH_3–O radical turned out to be significantly overestimated (by about 3.2 eV). As a consequence the O–H bond energies in alcohol molecules (CH_3OH, C_2H_5OH, etc) were greatly underestimated by about 2.7 eV. Therefore, to describe bond energies in alcohol molecules more accurately, we fit O–C bond energies with no neighbours on the oxygen side to CH_3O (−4.00 eV). Thus, we deliberately sacrificed the accuracy of bond energies for CO and CO_2 molecules to better predict C–O and O–H energies in alcohol molecules, because these, and their derivatives, are ultimately of more interest.

The dissociation energies of CH_4 into $CH_3 + H$ and CH_3CH_3 into two CH_3 fragments are shown because these bonds are important for the dissociation of larger H, C, O-containing molecules and because initially the REBO potential was designed to predict average hydrocarbon bond additive energies rather than bond dissociation energies [6]. The remaining bond dissociation energies are predictions for bonds that were not explicitly included in the fitting database. All together, differences between calculated values and the experimental data range from 2% for O_2 to 31% for CO_2. These discrepancies are, in general, slightly larger than the errors predicted for hydrocarbon molecules reported in table 5 and in [8]. This is because the transferability of bond dissociation energies among oxygen containing molecules is not as good as among pure hydrocarbon molecules.

3.2. Chemistry of gas-phase collisions

The chemical reactions considered involve small molecules that contain H, C, and O, or some combination thereof, including O_2, H_2, water (H_2O), methane (CH_4), methyl radical, ethane (CH_3CH_3), ethyl radical (CH_3CH_2), methanol (CH_3OH), ethanol (C_2H_5OH), 1-butanol (C_4H_9OH), 1-octanol ($C_8H_{17}OH$), ethyl ether ($C_2H_5OC_2H_5$), and n-butyl ether ($C_4H_9OC_4H_9$). The collisions occur in the gas phase by giving one molecule a translational velocity towards the other molecule. Incident kinetic energies range from 0.1 to 40 eV per molecule. In each case, the outcomes of 10 collisions from differing initial random molecular orientations are reported. It should be pointed out that the molecules have no angular momentum prior to the collisions. That is, all the atoms in the incident molecules initially have only translational velocities towards the target molecule. However, after the collisions, the translational kinetic energy not only alters the potential energy through chemical reactions, but portions of it are also transformed into vibrational and rotational modes. Snapshots from some representative collisions are shown in figure 5.

When O_2 collides with C_2 at incident energies of 0.1, 0.5, and 1.0 eV/O_2 molecule, the particles either elastically bounce off of each other if they are not favourably oriented with respect to one another, or a linear radical of ·C≡C–O–O· is formed if one C atom can get closer to only one of the O atoms. As the energy increases, the incidence of radical formation increases from 30% at 0.1 eV/O_2 molecule to 70% at 1.0 eV/O_2 molecule. While this linear radical would not be expected to be long lived, it is formed because of the high reactivity of the C_2 species and because the molecules do not have enough kinetic energy to react to form more stable molecules.

At 2.0 eV/O_2 molecule, 30% of the collisions produce ·C≡C–O· and an O· radical. These higher incident energies are enough to dissociate the O_2 molecule and allow the reactive C_2 to bond to one of the oxygen atoms. The rest of the trajectories produce elastic, nonreactive collisions. At incident energies of 3.0, 5.0, and 10 eV/O_2 molecule, two molecules of CO are produced in up to 40% of the collisions, which the rest of the collisions are elastic. Again, favourable alignment of the two particles is required to produce the CO. At incident energies between 10 and 50 eV/O_2 molecule, one or two CO molecules are produced from the

bond dissociations and subsequent reactions of O–O and C–C in every trajectory considered regardless of the relative molecular orientations.

Esterification is expected when an alcohol, CH_3OH, and a carboxylic acid, CH_3COOH, react and we try to induce an esterfication reaction between these two molecules through gas phase collisions. However, no reaction occurs until about 10 eV/CH_3OH molecule. At 20 and 30 eV/CH_3OH molecule, the CH_3OH remains unchanged and the carboxylic acid decomposes into stable fragments such as CO, CH_3, and OH for 50%–60% of collisions. At energies of 40 eV/CH_3OH molecule, the molecules collide more violently and produce a larger array of fragments, not all of which are stable on their own but all of which are reasonable products of high-energy collisions (see, for example, [18, 19]).

Additional gas-phase collisions are considered between O_2 and CH_3, CH_3CH_2 or CH_3CH_3. When O_2 collides with the reactive methyl and ethyl radicals at low incident energies, 20–90% of reactive conversion to products is observed. This finding depends heavily on the relative orientation of the molecules, however. For example, in the case of the O_2–CH_3 collision, the impact of one O with the C is compared, shown in figure 5, with the collision of the area between the two O atoms and the C atom (not shown). In the first case, CH_3–O–O is produced for 50–20% of collisions at low energy (0.1–10 eV/O_2 molecule) and there are no decompositions (such as $H + CH_2 + O_2$), or production of carboxyl radicals and molecules (such as CH_3O and CH_2O) as occurs at higher incident energies. In the case of O_2–CH_3CH_2 collisions, the same tendency is predicted, that is, CH_3CH_2OO is produced at low incident energies of 0.1–5.0 eV/O_2 molecule. This is because at low energies the C and O can sometimes line up with each other and impact gently enough to form a chemical bond.

In contrast, at high energies the collisions are too violent for a chemical bond to be sustained. In the cases of collisions between stable molecules, O_2 and CH_3CH_3, no reactions are produced up to 10 eV of incident energy per O_2 molecule. At higher energies than 10 eV/O_2 molecule, the decompositions of CH_3CH_3, or production of carboxyl radicals and molecules, such as CH_3O, CHO, CH_3OO, CH_3CH_2O, and CH_2O, occurs most of the time.

Collisions are also considered between H_2O and CH_3 or CH_3CH_2. H_2O is quite stable and does not react with methyl and ethyl radicals as a result of collisions at incident energies less than about 20 eV/H_2O molecule. The collisions of H_2O with CH_3 or CH_3CH_2 result in no new products except at incident energies greater than 10 eV/H_2O molecule. This can be explained by the fact that H_2O is less reactive than O_2 and high energies are required to cause dissociation. Some of the products that result from these high-energy collisions (e.g., 20 eV/H_2O molecule) are stable CH_3OH and CH_2O, and meta-stable CH_3O and CH_2OH.

After each gas-phase collision, the kinetic energy of the system usually decreases and the potential energy increases, except for the case where CO is produced from $O_2 + C_2$, which shows the opposite tendency. None of the collisions result in the formation of anomalous bonds that violate orbital theory. Monitoring the total energy of the system is one way of determining how well energy is conserved in the simulations, which is an indication of potential stability. The total energy of the reacting systems remains relatively constant ($\leqslant$0.1 eV) except for some high-energy collisions at 40–50 eV per molecule (CH_3COOH–CH_3OH, O_2–CH_4, O_2–CH_3CH_2, H_2O–CH_4, H_2O–CH_3CH_2, H_2O–CH_3CH_3) where the total energies change by up to about 0.4 eV for the system as a whole. Additionally, the total energy of the O_2–CH_3 collision changes by as much as 0.2 eV when the collision produces CH_3OO, which is metastable, at low impact energies, but changes by less than 0.05 eV at higher incident energies. Larger changes in the total energy thus are most likely to occur when there are substantial changes in the chemical bonding of the constituent molecules.

We explored the possibility that the observed non-conservation of energy as a result of high-impact collisions was caused by timesteps that were too large (at 0.2 fs) and considered

smaller timesteps as low as 0.02 fs. The only collision whose results changed with changes in the time step was the CH_3COOH–CH_3OH collision at 30 eV which produces $CH_2O + 2H$ at a time step of 0.1 fs instead of $CH_3 + O + H$ with 0.2 fs time step for the same relative molecular orientations.

4. Conclusions

The second-generation REBO potential, which is parametrized for hydrocarbons by Brenner *et al* [3], has been expanded to include covalent C–O, H–O, and O–O interactions in addition to the existing covalent C–C, C–H, and H–H interactions. Unlike force field models, this potential allows for chemical bond rupture and bond formation to occur. The expanded potential is therefore applied to some example applications, including the investigation of the stability and optimization of molecular and polymer chain structures composed of C, H, and O and the study of chemical reactions that result from gas-phase collisions of C, H, and O containing molecules. These tests show that the potential does a reasonably good job of describing the various molecular and polymeric structures considered here.

It should be noted that this potential is optimized for short-ranged covalent bonds. To increase its utility, future development will focus on the inclusion of long-range interactions through coupling to, e.g., Lennard-Jones potentials, and the inclusion of partial charges. The former extension will allow us to consider solid-state structures where, for example, van der Waals interactions are important, such as polymers, while the latter extension will allow us to consider structures where the bonding has significant ionic character.

Acknowledgments

We thank Donald Brenner for many helpful discussions. This work was supported by the National Science Foundation (CHE-020200838) and by the National Science Foundation-funded Network for Computational Nanotechnology (EEC-0228390).

References

[1] Brenner D W 1990 *Phys. Rev.* B **42** 9458
[2] Brenner D W 2000 *Phys. Status Solidi* b **217** 23
[3] Brenner D W, Shenderova O A, Harrison J A, Stuart S J, Ni B and Sinnott S B 2002 *J. Phys.: Condens. Matter* **14** 783
[4] Abell G C 1985 *Phys. Rev.* B **31** 6184
[5] Tersoff J 1986 *Phys. Rev. Lett.* **56** 632
[6] Tersoff J 1988 *Phys. Rev.* B **37** 6991
[7] Tersoff J 1988 *Phys. Rev. Lett.* **61** 2879
[8] Tersoff J 1989 *Phys. Rev.* B **39** 5566
[9] Mowrey R C, Brenner D W, Dunlap B I, Mintmire J W and White C T 1991 *J. Phys. Chem.* **95** 7138
[10] Taylor R S and Garrison B J 1995 *Langmuir* **11** 1220
[11] Garrison B J, Dawnkaski E J, Srivastava D and Brenner D W 1992 *Science* **255** 835
[12] Taylor R S and Garrison B J 1994 *J. Am. Chem. Soc.* **116** 4465
[13] Qi L and Sinnott S B 1997 *J. Phys. Chem.* B **101** 6883
[14] Qi L and Sinnott S B 1998 *J. Vac. Sci. Technol.* A **16** 1293
[15] Qi L and Sinnott S B 1998 *Surf. Sci.* **398** 195
[16] Qi L and Sinnott S B 1998 *Nucl. Instrum. Methods Phys. Res.* B **140** 39
[17] Plaisted T A, Ni B, Zahrt J D and Sinnott S B 2001 *Thin Solid Films* **381** 73
[18] Plaisted T A and Sinnott S B 2001 *J. Vac. Sci. Technol.* A **19** 262
[19] Wijesundara M B J, Hanley L, Ni B and Sinnott S B 2000 *Proc. Natl Acad. Sci. USA* **97** 23
[20] Wijesundara M B J, Ji Y, Ni B, Sinnott S B and Hanley L 2000 *J. Appl. Phys.* **88** 5004

[21] Hu Y, Shen S, Liu L, Jayanthi C S, Wu S-Y and Sinnott S B 2002 *J. Chem. Phys.* **116** 6738
[22] Harrison J A, Brenner D W, White C T and Colton R J 1991 *Thin Solid Films* **206** 213
[23] Harrison J A, White C T, Colton R J and Brenner D W 1992 *Surf. Sci.* **271** 57
[24] Harrison J A and Brenner D W 1994 *J. Am. Chem. Soc.* **116** 10399
[25] Perry M D and Harrison J A 1995 *J. Phys. Chem.* **99** 9960
[26] Perry M D and Harrison J A 1996 *Langmuir* **12** 4552
[27] Perry M D and Harrison J A 1997 *J. Phys. Chem.* B **101** 1364
[28] Ni B and and Sinnott S B 2001 *Surf. Sci.* **487** 87
[29] Robertson D H, Brenner D W and Mintmire J W 1992 *Phys. Rev.* B **45** 12592
[30] Yakobson B I, Brabec C J and Bernholc J 1996 *Phys. Rev. Lett.* **76** 2511
[31] Cornwell C F and Wille L T 1997 *Solid State Commun.* **101** 555
[32] Garg A, Han J and Sinnott S B 1998 *Phys. Rev. Lett.* **81** 2260
[33] Garg A and Sinnott S B 1999 *Phys. Rev.* B **60** 13786
[34] deSainteClare P, Son K, Hase W L and Brenner D W 1996 *J. Am. Chem. Soc.* **100** 1761
[35] Marks N A 2000 *Phys. Rev.* B **63** 035401
[36] Petukhov A V and Fasolino A 2000 *Phys. Status Solidi* a **181** 109
[37] Ishimaru M 2001 *J. Phys.: Condens. Matter* **13** 4181
[38] Petukhov A V, Passerone D, Ercolessi F, Tosatti E and Fasolino A 2000 *Phys. Rev.* B **61** R10590
[39] Que J-Z, Radny M W, Smith P V and Dyson A J 2000 *Surf. Sci.* **444** 123
[40] Que J-Z, Radny M W and Smith P V 2000 *Surf. Sci.* **444** 140
[41] Schofield S R, Radny M W and Smith P V 2000 *Phys. Rev.* B **62** 10199
[42] Que J-Z, Radny M W and Smith P V 1999 *Phys. Rev.* B **60** 8686
[43] Abrams C F and Graves D B 1999 *J. Appl. Phys.* **86** 5938
[44] Tanaka J, Abrams C F and Graves D B 2000 *Nucl. Instrum. Methods* B **18** 938
[45] Dyson A J and Smith P V 1996 *Surf. Sci.* **355** 140
[46] Jang I and Sinnott S B 2004 *J. Phys. Chem.* B at press
[47] Sinnott S B, Shenderova O A, White C T and Brenner D W 1998 *Carbon* **36** 1
[48] Stuart S J, Tutein A B and Harrison J A 2000 *J. Chem. Phys.* **112** 6472
[49] Frisch M J *et al* 2001 *Gaussian 98* Revision A.1x (Pittsburgh, PA: Gaussian)
[50] Lide D R 1990 *CRC Handbook of Chemistry and Physics* (Boca Raton, FL: CRC Press)
[51] Frenkel D and Smit B 1996 *Undestanding Molecular Simulation: From Algorithms to Applications* (San Diego, CA: Academic)
[52] Sutton L E 1958 *Tables of Inter-Atomic Distances* (London: Chemical Society) (Chemical Society Special Publication)
[53] Cottrell T L 1958 *The Strengths of Chemical Bonds* (London: Butterworths)